Central Lancashire Online Knowledge (CLoK)

Title	Investigating Ultra-Large Large-Scale Structures: Potential Implications for Cosmology
Type	Article
URL	https://clok.uclan.ac.uk/53142/
DOI	https://doi.org/10.1098/rsta.2024.0029
Date	2025
Citation	Lopez, Alexia, Clowes, Roger G orcid iconORCID: 0000-0001-8370-465X and Williger, Gerard M. (2025) Investigating Ultra-Large Large-Scale Structures: Potential Implications for Cosmology. Philosophical Transactions of the Royal Society A: Mathematical, Physical and Engineering Sciences, 383 (2290). ISSN 1364-503X
Creators	Lopez, Alexia, Clowes, Roger G and Williger, Gerard M.

It is advisable to refer to the publisher's version if you intend to cite from the work.
https://doi.org/10.1098/rsta.2024.0029

For information about Research at UCLan please go to http://www.uclan.ac.uk/research/

Author for correspondence:

Alexia M. Lopez

e-mail: missalexia.lopez@gmail.com

Investigating Ultra-Large Large-Scale Structures: Potential Implications for Cosmology

A. M. Lopez[1], R. G. Clowes[1] and G. M. Williger[2]

[1]Jeremiah Horrocks Institute, University of Central Lancashire, Preston, PR1 2HE, United Kingdom
[2]Department of Physics and Astronomy, University of Louisville, Louisville, KY 40292, USA

Large-scale structure (LSS) studies in cosmology map and analyse matter in the Universe on the largest scales. Understanding the LSS can provide observational support for the Cosmological Principle (CP) and the Standard Cosmological Model (ΛCDM).

In recent years, many discoveries have been made of LSSs that are so large that they become difficult to understand within ΛCDM. Reasons for this are: they potentially challenge the CP, (i.e. the scale of homogeneity); and their formation and origin are not fully understood.

In this article we review two recent LSS discoveries: the Giant Arc (GA, ~ 1 Gpc) and the Big Ring (BR, ~ 400 Mpc). Both structures are in the same cosmological neighbourhood — at the same redshift $z \sim 0.8$ and with a separation on the sky of only $\sim 12°$. Both structures exceed the often-cited scale of homogeneity (Yadav+ 2010), so individually and together, these two intriguing structures raise more questions for the validity of the CP and potentially hint at new physics beyond the Standard Model.

The GA and BR were discovered using a novel method of mapping faint matter at intermediate redshifts, interpreted from the Mg II absorption doublets seen in the spectra of background quasars.

1. Introduction

Large-scale structure (LSS) studies are motivated by the need for observational data to confirm the predictions of the Standard Cosmological Model (ΛCDM). In particular, from studying the LSS of matter on the very largest scales, one can learn about the growth of cosmic structure [1] and about the Universe's dynamical history [2], thus allowing comparison with ΛCDM. Furthermore, and of some current interest, LSS can test the assumption of large-scale homogeneity, which is a fundamental aspect of the Cosmological Principle (CP) and hence of the theoretical framework in cosmology.

Unfortunately, the CP lacks a precise and agreed definition. Different interpretations can be encountered in the cosmological literature and across the history of cosmology. The details can be vague. For example, the textbook version of the CP might say that the Universe on large scales is homogeneous and isotropic. However, what those large scales might be is often not clearly specified, and, indeed, the expectation of what is plausible seems to have increased by at least a factor of ten over the years.

Consider the following three interpretations of the CP, and specifically what is meant by homogeneity. (i) There exists some large scale, known as the scale of homogeneity on which the Universe can be smoothed and the distribution of matter would then be well represented by a stationary random process, e.g., [3–5]. (ii) The power spectrum suggests that there can always be some large scale at which statistically-significant deviations might be found in the matter distribution, but such deviations on large scales should be rare, e.g., [2,6]. (iii) There should be similarity everywhere (maximally symmetric). Any observed large-scale structuring indicates that the scale of homogeneity, if it exists, must then be larger than these scales. The occurrence of a particular LSS, even the largest known, does not imply that the *probability* of finding a comparable LSS elsewhere is any different. Points (ii) and (iii) could be contradictory, given that point (ii) suggests that the largest structures should be rare, and point (iii) suggests that the largest structures need not be a problem for the CP if their probabilities are homogeneous and isotropic. (How would we know that?) A useful overview of the various interpretations of the CP can be found in [7].

The diversity in the interpretation of homogeneity in the CP has led to differing conclusions on whether the observed matter supports a homogeneous Universe. For example, there have been claims that large-survey analysis supports homogeneity in luminous red galaxies and in quasars [8–10]. However, the accumulating set of ultra-large LSS (uLSS) [1] discoveries might indicate that homogeneity is not supported. For a recent list of the largest LSSs that appear to extend beyond Yadav's [4] estimated ~ 370 Mpc upper limit to the scale of homogeneity, see Table 1 in [11].

Perhaps individual uLSS discoveries can instead be explained by appealing to extreme-value statistics in some form. For example, [6] and [12] address the Sloan Great Wall (SGW) and the Huge Large Quasar Group (Huge-LQG) with mock catalogues and random catalogues respectively, finding that mock / random structures of comparable size and overdensity may be readily reproduced. Somewhat differently for the Huge-LQG, [13] used the Horizon Run 2 cosmological simulation and extreme-value analysis to show that the Huge-LQG is compatible with the standard ΛCDM model if it should happen to be the largest such structure in a volume over five times larger. Similarly, for the SGW, [6] found that, while structures comparable to the size and overdensity of the SGW were reproduced in their simulations, they were always in the top six largest and richest structures detected in the 200 mock samples.

These results from [6] and [13] suggest that, in the matter of the compatibility of uLSSs with the ΛCDM model, the *accumulated* set of uLSSs might be of more importance than any one individual structure.

In this review article we discuss two intriguing uLSS discoveries, the Giant Arc (GA) [11] and the Big Ring (BR) [14]. See Figure 1 for an artistic impression of both of these structures on

---

[1]We have introduced the new term 'ultra-large LSS' (uLSS) to denote those structures that exceed the Yadav estimated ~ 370 Mpc upper limit to the scale of homogeneity [4].

the sky. We summarise their method of discovery and statistical analysis, describe their observed properties, and comment or speculate on their possible origins. The GA and the BR are in the same cosmological neighbourhood, at $z \sim 0.8$ and separated by only $\sim 12°$ on the sky. Individually and together, they exceed the Yadav 370 Mpc scale, and thus may at least challenge some interpretations of the CP. (Note that the word 'challenge' is not synonymous with 'contradict', but it does imply something to be investigated further.) Their sizes and morphologies appear to be hard to explain in the standard ΛCDM model. Quite possibly, new developments in cosmology will follow from the continued investigation of intriguing and unexpected anomalies such as these.
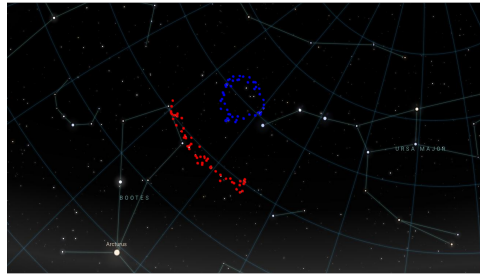

Figure 1: An approximate projection of the GA and BR visually-identified absorber members superimposed onto an image of the night sky taken from Stellarium. This figure gives an impression of the scale of the two uLSSs, their position on the sky and their proximity.

2. The Mg II Method

Observations for studying LSS in the Universe could be broadly divided into two categories: (a) observations of low-luminosity objects at low to intermediate redshifts (e.g., [15–17]); and (b) observations of high-luminosity objects at intermediate to high redshifts (e.g., [18–25]). There are benefits and challenges to both categories. In category (a), photometric redshifts, for very large numbers of objects, are commonplace, but the large redshift errors can lead to blurring of structures along the line of sight. Spectroscopic redshifts, generally for smaller numbers of objects, are more demanding of telescope time, and are more likely to feature in category (b). The redshift errors are then smaller but may still be associated with some blurring.

A novel method for analysing LSS is to infer the low-luminosity matter at intermediate redshifts from the presence of sharp metal absorption lines in the spectra of high-redshift quasars. The Mg II doublet, specifically, arises from low-ionised metal-enriched gas which is well-known to trace star formation regions [26–30]. From many quasar observations covering a large area of sky, such as the SDSS footprint or the recent DESI survey footprint (at the time of writing this is not yet publicly available), one can then map the inferred, low-luminosity, intervening matter at intermediate redshifts and learn about the LSS.

The sources of data for the Mg II method are these. The first-order data are the spectroscopic quasar observations from the Sloan Digital Sky Survey (SDSS) quasar catalogues. For previous work (including the discovery and analysis of the GA) we used the 'cleaned' quasar catalogues DR7QSO [31] and DR12Q [32]. For recent work (including the discovery and analysis of the BR) we used the newer 'cleaned' DR16Q quasar catalogue [33]. The second-order data are the corresponding Mg II catalogues from independent authors. For the Mg II absorber catalogues corresponding to DR7QSO and DR12Q we downloaded the Zhu and Ménard (Z&M) [34] data,

and for the absorber catalogues corresponding to DR16Q we downloaded the Anand et al. (Anand21) [35] data.

3. Statistical Analysis

In this section we summarise the statistical analyses performed on the GA and BR to assess them, sub-divided by the different statistical tests used. Full details can been found in the respective papers.

(a) Power Spectrum Analysis

The 2D Power Spectrum Analysis (2D PSA) [36,37] is a powerful statistical tool for detecting clustering of sources in a rectangular field using Fourier methods. The 2D PSA has the power to detect the scale of clustering as well as its statistical significance on that scale. We applied this test to the field containing the GA. Given that the (likely) dominant feature of clustering in the GA field was the GA itself, we reduced the typical Mg II image size, mostly along the north-south axis (Figure 2), before applying the 2D PSA.
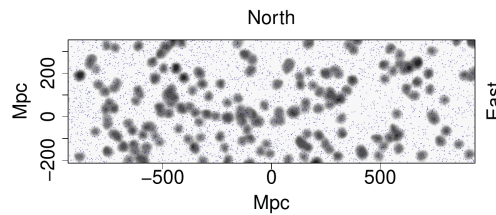

Figure 2: The tangent-plane distribution of Mg II absorbers centred on the GA in the redshift slice $z = 0.802 \pm 0.060$ using the Z&M data. The grey contours, increasing by a factor of two, represent the density distribution of the absorbers which have been smoothed using a Gaussian kernel of $\sigma = 11$ Mpc, and flat-fielded with respect to the distribution of background probes (quasars). The dark blue dots represent the background probes. This figure corresponds to Figure 9a of the GA paper.

In Figure 3 we are showing the 2D PSA statistic Q' corresponding to the GA field seen in Figure 2. The (six) high points towards the left of the figure allow a clustering scale of $\lambda_c \sim 270$ Mpc to be identified. The final PSA statistic Q for this scale λ_c corresponds to a detection of clustering at a significance of 4.8σ. Given the clustering scale of $\lambda_c \sim 270$ Mpc, this is likely detecting the width of the GA as perceived along its length.

(b) Cuzick and Edwards Test

The Cuzick and Edwards (CE) test [38] is a case-control k (or q here) nearest-neighbours algorithm, originally intended to assess geographical, spatial clustering of medical illnesses in inhomogeneous populations. Given the complications of the data we work with — the possible inhomogeneity of the quasars (the probes) available for detecting intervening Mg II absorbers — we applied this test to both the GA and the BR.

Cuzick and Edwards found the test to be most powerful when the ratio of controls to cases is between 4 and 6. However, for the GA field there were ~ 20 times as many probes (controls) as Mg II absorbers (cases), and for the BR field there were ~ 50 times as many probes as Mg II absorbers. For the CE test calculation, in both cases of the GA and BR, a subset of probes was
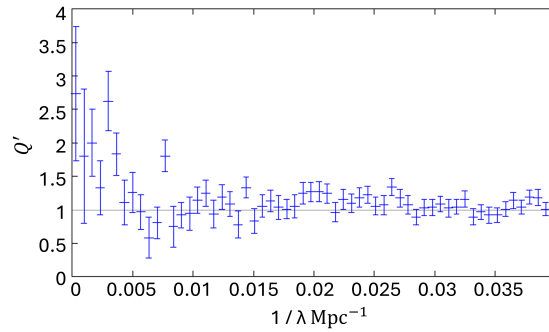
Figure 3: The 2D PSA test statistic Q' as a function of clustering scale $1/\lambda$ with λ in Mpc. The bin size is 6.7×10^{-4} Mpc^{-1} and the error bars are $\pm\sigma$. The horizontal line $Q' = 1$ indicates the expectation value in the case of no clustering. The (six) high points towards the left of the plot allow a clustering scale of $\lambda_c \sim 270$ Mpc to be identified. The final PSA statistic Q for this scale λ_c corresponds to a detection of clustering at a significance of 4.8σ. This figure corresponds to Figure 13 in the GA paper.

randomly selected to reduce the ratio of controls to cases to $5 : 1$, and this procedure was then repeated 100 times. Within each run of randomly selected probes, the CE test was run with 2000 simulations.

For the GA field, seen in Figure 2, the CE test found significant $p = 0.0027$ field clustering at $q = 40$ (see Figure 4a), corresponding to a significance of 3.0σ. For the (reduced) BR field seen in Figure 5, the CE test did not find conclusive significant clustering. In Figure 4b the p-value drops below 0.05 (indicated by the blue, horizontal line), reaching a minimum of $p = 0.043$ (1.7σ) at $q = 58$.

(c) FilFinder algorithm

The FilFinder algorithm [39] is a 2D filament identification tool, originally designed to trace filamentary structure in small gaseous regions, such as the ISM and star-formation regions [40–42]. We applied it to the field containing the BR to objectively trace the longest and most-connected filaments in the field. Figure 6a shows the FilFinder algorithm applied to the BR field (for details of the parameter choices, see the original discovery paper). By incrementally increasing the size threshold of the algorithm, it removes the smaller and less connected filaments (see Figure 6b). In doing so, only the filament tracing the BR remained. Applying the FilFinder algorithm to the BR field shows that the BR is the most connected and largest filament in the field.

(d) Single Linkage Hierarchical Clustering Algorithm

The Single-Linkage Hierarchical Clustering (SLHC) algorithm is equivalent to a Minimal Spanning Tree (MST) when the MST is separated at a specified linkage scale. When applied to 3D spatial data the SLHC algorithm determines the candidate (algorithmic) 'structures' within the dataset. The linkage scale will determine the set of data points included in a candidate structure. Naturally, the choice of linkage scale must be related to the field density: in a high-density region, the chosen linkage scale should be smaller than in a low-density region. We adopt the GA field as a standard field (linkage scale s_0, density ρ_0) and use the relation $s = (\rho_0/\rho)^{1/3} s_0$ to obtain the linkage scale s for any other field of density ρ.

The SLHC algorithm identified the majority of the absorbers belonging to the visually-identified GA (using the older Z&M database) in two agglomerations: a large, statistically-significant portion and a smaller, not statistically-significant portion, which were named GA-main
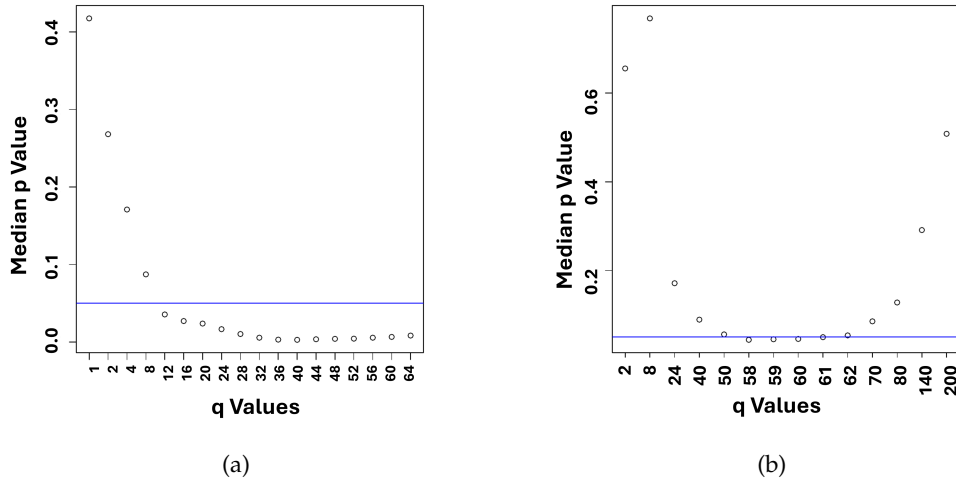
(a)   (b)

Figure 4: (a) The median p-value over 100 runs of 2000 simulations as a function of chosen q value. These results correspond to the GA field seen in Figure 2. The p-value reaches a minimum of $p = 0.0027$ (corresponding to a 3σ detection) at $q = 40$. These results are based on data from the older Z&M database. The x-axis labels are: $1, 2, 4, 8, 12, 16, 20, 24, 28, 32, 36, 40, 44, 48, 52, 56, 60, 64$. (b) The median p-value over 100 runs of 2000 simulations as a function of chosen q value. These results correspond to the BR field seen in Figure 5. The p-value reaches a minimum of $p = 0.043$ at $q = 58$. These results are based on data from the Anand21 database. The x-axis labels are $2, 8, 24, 40, 50, 58, 60, 61, 62, 70, 80, 140, 200$.
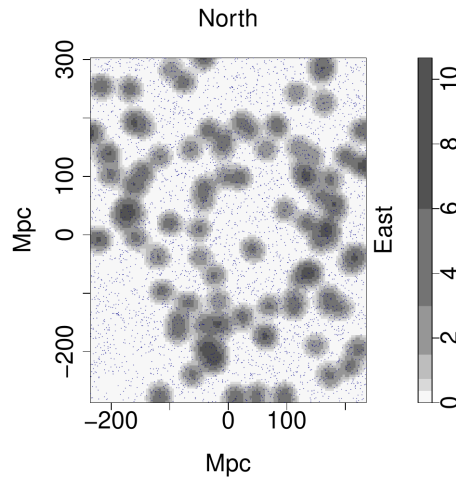

Figure 5: The tangent-plane distribution of Mg II absorbers centred on the BR in a reduced field size in the redshift slice $z = 0.802 \pm 0.060$ using the Anand21 data. The grey contours represent the density distribution of the absorbers which have been smoothed using a Gaussian kernel of $\sigma = 11$ Mpc, and flat-fielded with respect to the distribution of background probes (quasars). The key on the right-hand side shows the relative density of the Mg II absorbers, which are increasing by a factor of two. The dark blue dots represent the background probes.
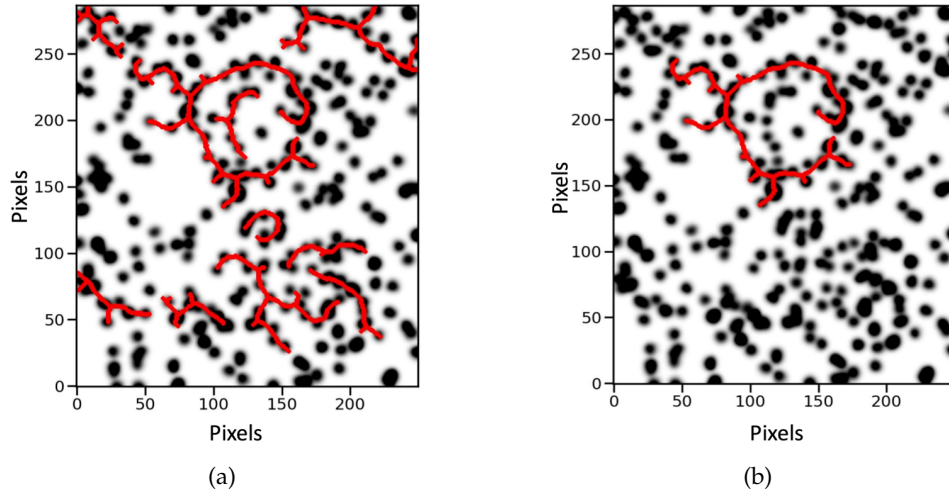
Figure 6: (a) Filaments, shown in red, identified by the FilFinder algorithm in the BR field. (b) Starting from (a), the FilFinder size threshold parameter was incrementally increased, leaving only the filament that traces the absorbers belonging to the BR. The Mg II data are from the Anand21 database.

and GA-sub, respectively. The two GA agglomerations visually overlapped on the sky, indicating that they could belong to the same candidate structure if given a more complete survey coverage. (Recall that the background quasars are responsible for the detection of intervening Mg II systems.) The statistical significance of GA-main was then calculated using the Convex Hull of Member Spheres (see originally [43] and the corresponding GA or BR paper for more details). The CHMS statistical significance of GA-main was 4.53σ. The overdensity of GA-main was calculated both with the CHMS method and the Pilipenko MST-overdensity method [44]. The CHMS-overdensity and MST-overdensity for GA-main were $\delta\rho_{CHMS}/\rho = 0.9 \pm 0.6$ and $\delta\rho_{MST}/\rho = 1.3 \pm 0.3$ respectively. Clearly, the larger error estimates from the CHMS-overdensity indicate that those results should be taken with caution. A mass excess was estimated from the MST-overdensity by assuming that $\delta_n = \delta_m$, where δ_n is the MST-overdensity and δ_m is the mass overdensity. We took the critical density of the Universe to be 9.2×10^{-27} kg m^{-3}. The estimated mass excess for GA-main was $1.8 \times 10^{18} M_\odot$.

The SLHC algorithm applied to the BR field identified the majority of the absorbers belonging to the visually-identified BR (using the Anand21 database) in five, adjacent or overlapping, candidate structures, which, individually, were not statistically significant (see Figure 7, also see Figure 8 for our selection of the visually-identified BR). Similar to what was seen with the SLHC algorithms on the GA field, the individual candidate structures in the BR appear connected on the sky, indicating that they could belong to the same structure. Additionally, the results from the FilFinder add further support to the connectivity of the BR. We then apply the CHMS and MST significance tests to four versions of the BR: those identified by the FilFinder algorithm (FilFinder-identified); those identified by the SLHC in five candidate structures (SLHC-identified); the visually-identified absorbers making the circumference of the BR (BR-only); the visually-identified absorbers of the BR and everything contained within the BR (BR-all). Table 1 presents the results of the CHMS and MST significances applied to the four versions of the BR.

In Table 1, looking across the four versions in the CHMS significance calculations, the likely upper-limit estimate is from the visually-identified BR-all absorbers, and the lower-limit estimate is from the FilFinder-identified absorbers. This variation is expected, as the CHMS draws a unique volume around the absorber members, and empty volumes existing between absorbers will also
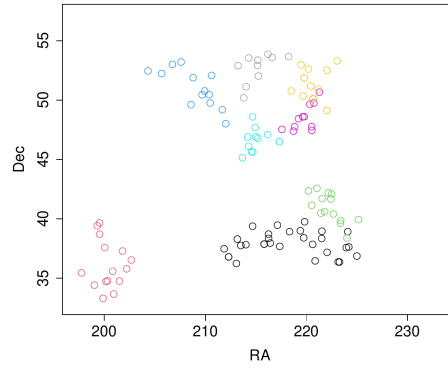
Figure 7: Eight of the 10 highest membership candidate structures identified by the SLHC algorithm applied to the BR field in the redshift slice $z = 0.802 \pm 0.060$. The colours represent the memberships which are ordered from high to low in the following way: black, red, green, blue, turquoise, pink, yellow, grey. In this figure, only the black points, representing absorbers belonging to the GA, are statistically significant. Data points are from the Anand21 database.
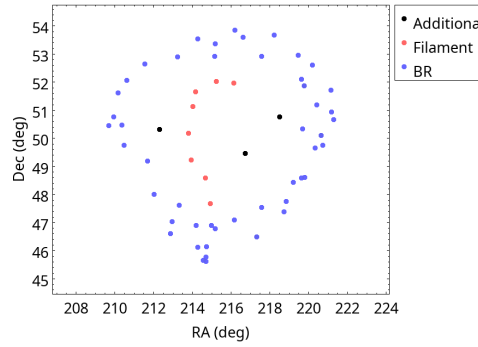

Figure 8: The visually-identified BR shown in blue points. The orange points mark an interesting filament running through the BR and the black points are the additional absorbers encompassed by the BR. Data points are from the Anand21 database.

Table 1: The SLHC and MST significance results applied to the four versions of the BR from the: SLHC-identified absorbers, visually-identified (BR-all and BR-only) absorbers and FilFinder-identified absorbers. These results are based on data from the Anand21 database.

	SLHC (σ)	Visual BR-all (σ)	Visual BR-only (σ)	FilFinder (σ)	**Mean** (σ)
CHMS	3.6	5.2	3.3	2.5	3.7 ± 1.1
MST	4.7	4.1	4.0	3.6	4.1 ± 0.5

be included. So, with large, empty volumes incorporated by the CHMS algorithm, the volume of a filamentary-type structure will be overestimated, and the significance of the unique CHMS volume will be correspondingly underestimated. For example, compare the filament-identified absorbers in Figure 6b with the visually-identified absorbers in Figure 8. The filament-identified absorbers envelop a large, empty region in the middle, as well as creating additional empty regions from the additional spurs to the north-west, whereas the visually-identified absorbers,

including all of those absorbers contained within the visually-identified BR, have fewer empty regions. The differences are then reflected in the CHMS significance estimates. Ideally, the CHMS algorithm is more appropriately used for clumpy, globular-type structures, and is less applicable to filamentary-type structures.

In contrast, in Table 1 the MST-significance values are less varying than the CHMS-significance values, as was also the case for the GA (see above). The CHMS algorithm relies on the unique volume encompassing the absorber members, whereas the MST calculation relies on the mean MST edge length between absorber members, which might be better suited for filamentary structures than the CHMS.

4. Observational Properties

In this section we give examples of and review some of the observational properties of the GA and the BR; further details can be found in the respective papers.

(a) Independent Corroboration

We used the SDSS DR16Q quasars and the DESI cluster catalogue from [45] to provide independent corroboration of the Mg II structures.

We used coloured contours superimposed on the Mg II images to visually inspect the relationship between the independent datasets. In Figures 9a and 9b we are seeing two examples of independent corroboration of the Mg II with the DR16Q field quasars and the DESI clusters, respectively. Visually, the coloured contours show a tendency to follow the grey contours, and since the quasars and DESI clusters are independent sources, they both provide independent corroboration of the GA and BR.

(b) The Proximity of the BR to the GA

The BR discovery is particularly interesting as it was made directly after the discovery of the GA but using the newer Anand21 Mg II catalogues instead of the older Z&M catalogues. The BR was first apparent when looking at the GA field with the Anand21 database; just to the north of the GA was an interesting ring shape, which we then investigated further.

On the sky, the GA and the BR are separated by only about $12°$, and they both lie in exactly the same redshift slice $z = 0.802 \pm 0.060$. Figure 1 is an approximate projection of the BR and GA absorber members imprinted onto a night sky image taken from Stellarium.

The direct discovery of a second uLSS, the BR, in the same cosmological neighbourhood as the first discovery, the GA, leads to the question of whether we would expect to find many more interesting, huge structures with circular or other conic-section morphologies. Perhaps, a more important question would be to determine *a priori* (i) whether ΛCDM can explain the occurrence of such huge structures, and (ii) whether, with the CP assumed, we should expect to find no other, or many more, of these types of structures.

(c) Hints of an Extended GA

In the BR field of the Anand21 databases there was also an interesting thin filament which appears to be a potential continuation of the GA. In Figure 10 we have added the GA points from the Z&M catalogues on the same plot as the BR points from the Anand21 catalogues. In addition we have added the points of the interesting thin filament that appeared in the Anand21 catalogues. With fitted ellipses it can be seen that if (with more data) this interesting filament was a continuation of the GA, then the GA, or Giant Ring (GR) would then encompass the BR.
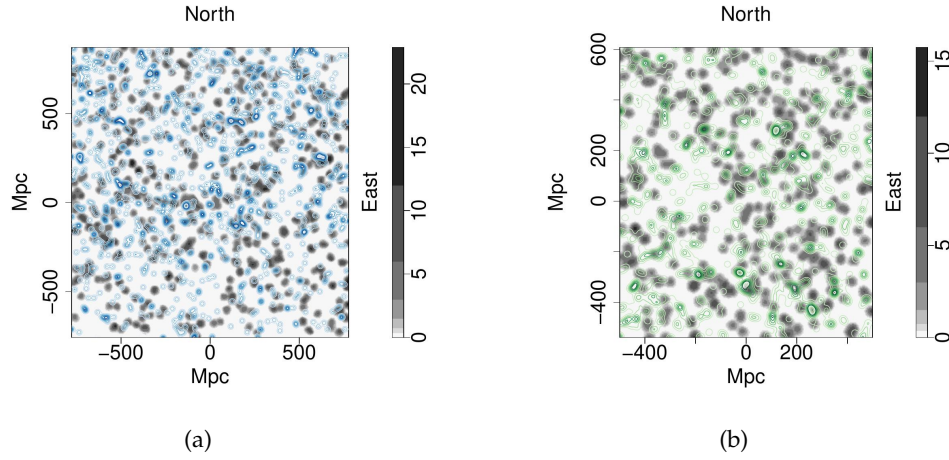
Figure 9: (a) Density distribution of the flat-fielded Mg II absorbers in the GA field in the redshift slice $z = 0.802 \pm 0.060$ represented by grey contours which have been smoothed using a Gaussian kernel of $\sigma = 11$ Mpc and flat-fielded with respect to the background probes (background quasars). The blue contours represent the *field* quasars from DR16Q — i.e., the quasars that are in the same field and redshift slice as the Mg II absorbers — which have been restricted to $i \leq 20.0$ and have also been smoothed with a Gaussian kernel of $\sigma = 11$ Mpc. The GA can be seen stretching ~ 1 Gpc across the field at the tangent-plane y-coordinate ~ 0. This figure corresponds to Figure 14(a) in the GA paper. (b) Density distribution of the flat-fielded Mg II absorbers in the BR field in the redshift slice $z = 0.802 \pm 0.060$ represented by grey contours which have been smoothed using a Gaussian kernel of $\sigma = 11$ Mpc and flat-fielded with respect to the background probes (background quasars). The green contours represent the DESI clusters that are in the same field and redshift slice as the Mg II absorbers, which have been restricted to a richness limit $R \geq 22.5$, and have also been smoothed with a Gaussian kernel of $\sigma = 11$ Mpc. The BR can be seen centred approximately on tangent-plane x, y coordinates $\sim (50, 300)$. In both figures, the key on the right-hand side shows the relative density of the Mg II absorbers, which are increasing by a factor of two.
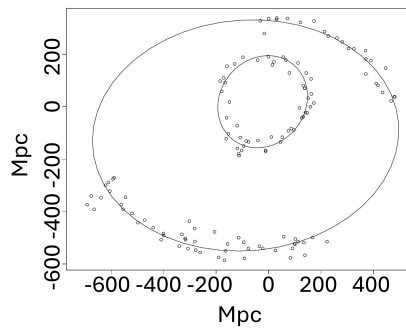

Figure 10: The GA points from Z&M (along the bottom) plotted with the BR points from Anand21 (in the middle). The thin filament to the north was also detected in the newer Anand21 catalogues. With the fitted ellipses it appears that the interesting thin filament could be a continuation of the GA, and if so, then this Giant Ring would encompass the BR.

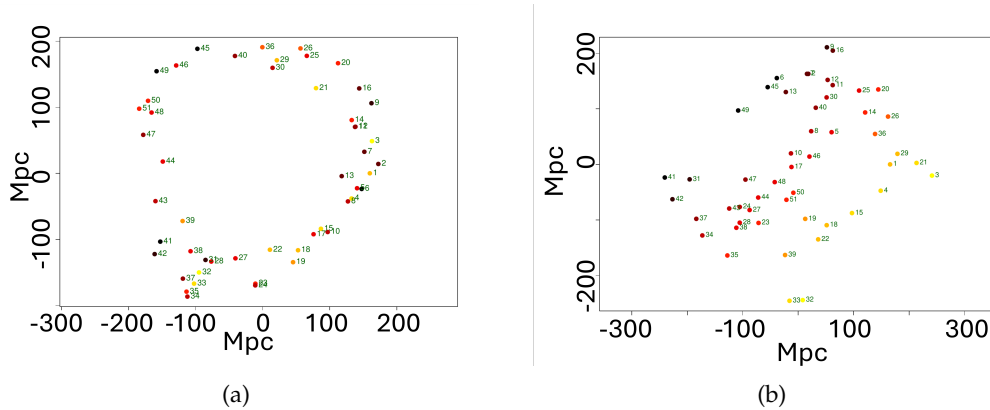(a)   (b)

Figure 11: (a) The BR absorber members projected onto a plane that resembles the original line-of-sight projection. (b) The BR absorber members projected onto a plane that resembles viewing the BR from a south-east direction. In this figure, the BR appears to resemble a coil shape. In both figures, the colours represent the redshifts of the absorbers, with nearer-z absorbers being lighter in colour and further-z absorbers being darker. The small numbers paired with each data point indicate their unique ID number.

(d) The 3D distribution of the BR

For the BR, we define a 3D coordinate system so that the distribution of Mg II absorber points in BR can be projected onto different planes, allowing for the investigation of the BR at different viewing angles.

In Figure 11a we are seeing the BR projected onto a plane, where the 3D coordinate system has been defined to resemble the original line-of-sight projection. The absorber points are numbered $1 - 51$, and these values are fixed to their absorber points through all rotations of the plane. The colours represent the redshift distribution, with nearer-z absorbers being lighter in colour and further-z absorbers being darker.

In Figure 11b we are next seeing the BR absorber points projected onto a plane that corresponds to viewing the BR from the south-east direction. From this viewing angle, the BR appears to resemble a coil shape. There also appear to be three distinct redshift bands, which were similarly seen from a side-on viewing angle (see the BR paper).

A 3D visualisation tool was also used to move around the BR absorber points to investigate the 3D structure. Using this tool also supported the coil-nature of the BR and it gave an impression of the near-z absorbers 'looping' into the central-z absorbers. The central-z absorbers then contained the majority of the BR absorbers and created the main ring shape in a thin, flat region. The far-z absorbers showed less continuity, with the appearance resembling a broken ring shape.

5. Discussion and Conclusions

We have reviewed two recently-discovered uLSSs: the Giant Arc and the Big Ring (GA and BR). Both were discovered visually as prominent overdensities in Mg II images, and subsequently supported by a range of statistical assessments and by independent corroboration from DR16Q quasars and DESI clusters. Both exceed the Yadav estimated upper-limit to the scale of homogeneity and add to an accumulating list of uLSSs that challenge the Cosmological Principle (CP) in this respect. We note that interpretations of the CP vary, however.

The GA and BR have intriguing morphologies, as indicated by their names. There is even a hint that the GA could extend into a Giant Ring that envelops the BR. While the BR appears entirely

as a ring in projection on the sky, in 3D visualisations it appears to coil into and out of a central flat ring (which contains most of the member absorbers).

Extreme-value analysis and cosmological simulations have shown that some individual occurrences of uLSSs may be consistent with the CP and with ΛCDM, but it is not obvious that the entire accumulating set of uLSSs will be consistent.

Given their morphologies, perhaps the GA and BR in particular require an explanation outside ΛCDM. One possibility might be cosmic strings, which have become of topical interest in recent work [46–53]. For the BR specifically, we noted its similarity in projection and radius to an individual baryonic acoustic oscillation (BAO) [54–58]. However, given the non-spherical, coiling nature of the BR, and its actually being larger than a BAO ($r \sim 200$ Mpc compared with $r \sim 150$ Mpc for a BAO), the BR having an origin in BAOs is probably ruled out.

Unexpected and apparently anomalous discoveries in cosmology, such as uLSSs in general and the GA and BR in particular, may be indicating a route to further understanding and to refinements of the standard model. It may be productive to see where they lead.

References

1. Huterer D, 2023 Growth of cosmic structure, *Astron. Astrophys. Rev.* **31**, 2. (doi:10.1007/s00159-023-00147-4)
2. Chow-Martínez M, Andernach H, Caretta CA, Trejo-Alonso JJ, 2014 Two new catalogues of superclusters of Abell/ACO galaxy clusters out to redshift 0.15. *Mon. Not. R. Astron. Soc.* **445**, 4073–4085. (doi:10.1093/mnras/stu1961)
3. Peebles PJE, 1993 *Principles of Physical Cosmology.* Princeton: Princeton University Press.
4. Yadav JK, Bagla JS, Khandai N, 2010 Fractal dimension as a measure of the scale of homogeneity. *Mon. Not. R. Astron. Soc.* **405**, 2009–2015. (doi:10.1111/j.1365-2966.2010.16612.x)
5. Aluri PK *et al.* 2023 Is the observable Universe consistent with the cosmological principle? *Class. Quantum Grav.* **40**, 094001. (doi:10.1088/1361-6382/acbefc)
6. Park C, Choi Y-Y, Kim J, Gott III JR, Kim SS, Kim K-S, 2012 The challenge of the largest structures in the Universe to cosmology. *Astrophys. J. Lett.* **759**, L7. (doi:10.1088/2041-8205/759/1/L7)
7. Schwarz DJ, 2010 *Thoughts on the Cosmological Principle.* in *Fundamental interactions: a memorial volume for Wolfgang Kummer.* World Scientific Publishing Co. Pte. Ltd. (doi:10.1142/9789814277839_0015)
8. Andrade U, Gonçalves RS, Carvalho GC, Bengaly CAP, Carvalho JC, Alcaniz J, 2022 The angular scale of homogeneity with SDSS-IV DR16 luminous red galaxies. *J. Cosmol. Astropart. Phys.* **2022**, 088. (doi:10.1088/1475-7516/2022/10/088)
9. Gonçalves RS, Rodrigo S, Carvalho GC, Andrade U, Bengaly CAP, Carvalho JC, Alcaniz J, 2021 Measuring the cosmic homogeneity scale with SDSS-IV DR16 quasars. *J. Cosmol. Astropart. Phys.* **2021**, 029. (doi:10.1088/1475-7516/2021/03/029)
10. Gonçalves RS, Carvalho GC, Bengaly CAP, Carvalho JC, Alcaniz JS, 2018 Measuring the scale of cosmic homogeneity with SDSS-IV DR14 quasars. *Mon. Not. Roy. Astron. Soc.* **481**, 5270–5274. (doi:10.1093/mnras/sty2670)
11. Lopez AM, Clowes RG, Williger GM, 2022 A Giant Arc on the sky. *Mon. Not. Roy. Astron. Soc.* **516**, 1557–1572. (doi:10.1093/mnras/stac2204)
12. Nadathur S, 2013 Seeing patterns in noise: gigaparsec 'structures' that do not violate homogeneity. *Mon. Not. Roy. Astron. Soc.* **434**, 398–406. (doi:10.1093/mnras/stt1028)
13. Marinello GE, Clowes RG, Campusano LE, Williger GM, Söchting IK, Graham MJ, 2016 Compatibility of the large quasar groups with the concordance cosmological model. *Mon. Not. Roy. Astron. Soc.* **461**, 2267–2281. (doi:10.1093/mnras/stw1513)
14. Lopez AM, Clowes RG, Williger GM, 2024 A Big Ring on the sky. (doi:10.48550/arXiv.2402.07591)

15. Geller MJ, Huchra JP, 1989 Mapping the Universe. *Science* **246**, 897–903. (doi:10.1126/science.246.4932.897)

16. Gott III JR, Jurić M, Schlegel D, Hoyle F, Vogeley M, Tegmark M, Bahcall N, Brinkmann J, 2005 A map of the Universe. *Astrophys. J.* **624**, 463–484. (doi:10.1086/428890)

17. Pomarède D, Tully RB, Graziani R, Courtois HM, Hoffman Y, Lezmy J, 2020 Cosmicflows-3: the South Pole Wall. *Astrophys. J.* **897**, 133. (doi:10.3847/1538-4357/ab9952)

18. Webster A, 1982 The clustering of quasars from an objective-prism survey. *Mon. Not. Roy. Astron. Soc.* **199**, 683–705. (doi:10.1093/mnras/199.3.683)

19. Crampton D, Cowley AP, Hartwick FDA, 1987 The space distribution of faint quasars from the CFHT survey. *Astrophys. J.* **314**, 129. (doi:10.1086/165045)

20. Crampton D, Cowley AP, Hartwick FDA, 1989 Redshifts of quasars in the CFGT/MMT survey: futher evidence for isolated groups. *Astrophys. J.* **345**, 59. (doi:10.1086/167881)

21. Clowes RG, Harris KA, Raghunathan S, Campusano LE, Söchting IK, Graham MJ, 2013 A structure in the Universe at $z \sim 1.3$ that exceeds the homogeneity scale of the R-W concordance cosmology. *Mon. Not. Roy. Astron. Soc.* **429**, 2910–2916. (doi:10.1093/mnras/sts497)

22. Horváth I, Hakkila J, Bagoly Z, 2014 Possible structure in the GRB sky distribution of redshift two. *Astron. Astrophys.* **561**, L12. (doi:10.1051/0004-6361/201323020)

23. Horváth I, Bagoly Z, Hakkila J, Tóth LV, 2015 New data support the existence of the Hercules-Corona Borealis Great Wall. *Astron. Astrophys.* **584**, A48. (doi:10.1051/0004-6361/201424829)

24. Balázs LG, Bagoly Z, Hakkila JE, Horváth I, Kóbori J, Rácz II, Tóth LV, 2015 A giant ring-like structure at $0.78 < z < 0.86$ displayed by GRBs. *Mon. Not. Roy. Astron. Soc.* **452**, 2236–2246. (doi:10.1093/mnras/stv1421)

25. Balázs LG, Rejtö L, Tusnády G, 2018 Some statistical remarks on the Giant GRB Ring. *Mon. Not. Roy. Astron. Soc.* **473**, 3169–3179. (doi:10.1093/mnras/stx2550)

26. Bergeron J, 1988 Galaxies giving rise to Mg II absorption systems in quasar spectra. *Proceedings of the 130th symposium of the International Astronomical Union* on *Large scale structures of the Universe*. **130**, 343.

27. Steidel CC, Sargent WLW, 1992 Mg II absorption in the spectra of 103 QSOs: implications for the evolution of gas in the high-redshift galaxies. *Astrophys. J. Suppl. S.* **80**, 1–108. (doi:10.1086/191660)

28. Churchill CW, Kacprzak GG, Steidel CC, 2005 Mg II absorption through intermediate redshift galaxies. *Proceedings of the IAU Colloquium 199* on *Probing Galaxies through Quasar Absorption Lines*. (doi:10.1017/S1743921305002401)

29. Kacprzak GG, Churchill CW, Steidel CC, Murphy MT, 2008 Halo gas cross sections and covering fractions of Mg II absorption selected galaxies. *Astro. J.* **135**, 922–927. (doi:10.1088/0004-6256/135/3/922)

30. Barnes LA, Garel T, Kacprzak GG, 2014 Ly-α and Mg II as probes of galaxies and their environments. *Publ. Astron. Soc. Pac.* **126**, 969–1009. (doi:10.1086/679178)

31. Schneider DP *et al.* 2010 The Sloan Digital Sky Survey quasar catalog. V. Seventh data release. *Astron. J.* **139**, 2360–2373. (doi:10.1088/0004-6256/139/6/2360)

32. Pâris I *et al.* 2017 The Sloan Digital Sky Survey quasar catalog: Twelfth data release. *Astron. Astrophys.* **597**, A79. (doi:10.1051/0004-6361/201527999)

33. Lyke BW *et al.* 2017 The Sloan Digital Sky Survey quasar catalog: sixteenth data release. *Astrophys J. Suppl.* **250**, 8. (doi:10.3847/1538-4365/aba623)

34. Zhu G, Ménard B, 2013 The JHU-SDSS metal absorption line catalog: redshift evolution and properties of Mg II absorbers. *Astrophys. J.* **770**, 130. (doi:10.1088/0004-637X/770/2/130)

35. Anand A, Nelson D, Kauffmann G, 2021 Characterizing the abundance, properties, and kinematics of the cool circumgalactic medium of galaxies in absorption with SDSS DR16. *Mon. Not. Roy. Astron. Soc.* **504**, 65–88. (doi:10.1093/mnras/stab871)

36. Webster AS, 1976a The clustering of radio sources–I: the theory of power-spectrum analysis. *Mon. Not. Roy. Astron. Soc.* **175**, 61–70.

37. Webster AS, 1976b The clustering of radio sources–II: the 4C, GB and MC1 surveys. *Mon. Not. Roy. Astron. Soc.* **175**, 71–83

38. Cuzick J, Edwards R, 1990 Spatial clustering for inhomogeneous populations. *J. Roy. Stat. Soc.* **52**, 73–104.

39. Koch EW, Rosolosky EW, 2015 Filament identification through mathematical morphology. *Mon. Not. Roy. Astron. Soc.* **452**, 3435–3450. (doi:10.1093/mnras/stv1521)

40. Mookerjea B, Veena VS, Güsten R, Wyrowski F, Lasrado A, 2023 Spiral structure and massive star formation in the hub filament-system G326.27-0.49. *Mon. Not. Roy. Astron. Soc.* **520**, 2517–2533. (doi:10.1093/mnras/stad215)

41. Zhang S *et al.* 2023 ATOMS: ALMA three-millimeter observations of massive star-forming regions - XIII. Ongoing triggered star formation within clump-fed scenario found in the massive (1500 M⊙) clump. *Mon. Not. Roy. Astron. Soc.* **520**, 322–352. (doi:10.1093/mnras/stad011)

42. Meidt SE *et al.* 2023 PHANGS-JWST first results: interstellar medium structure on the turbulent Jeans scale in four disk galaxies observed by JWST and the Atacama large millimeter/submillimeter array. *Astrophys. J. Lett.* **944**, L18. (doi:10.3847/2041-8213/acaaa8)

43. Clowes RG, Campusano LE, Graham MJ, Söchting IK, 2012 Two close large quasar groups of size ∼ 350 Mpc at $z \sim 1.2$. *Mon. Not. Roy. Astron. Soc.* **419**, 556–565. (doi:10.1111/j.1365-2966.2011.19719.x)

44. Pilipenko SV, 2007 The space distribution of quasars. *Astron. Rep.* **51**, 820–829. (doi:10.1134/S106377290710006X)

45. Zou H, Gao J, Xu X, Ma J, Zhou Z, Zhang T, Nie J, Wang J, Zue S, 2021 Galaxy clusters from the DESI legacy imaging surveys. I. Cluster detection. *Astrophys. J. Suppl. Ser.* **253**, 56. (doi:10.3847/1538-4365/abe5b0)

46. Ahmed W, Chowdhury TA, Nasri S, Saad S, 2023 Gravitational waves from metastable cosmic strings in Pati-Salam model in light of new pulsar timing array data. *Phys. Rev. D* **109**, 015008. (doi:10.1103/PhysRevD.109.015008)

47. Cyr B, Chluba J, Acharya SK, 2023 A cosmic string solution to the radio synchrotron background. (doi:10.48550/arXiv.2308.03512)

48. Ellis J, Lewicki M, Lin C, Vaskonen V, 2023 Cosmic superstrings revisited in light of NANOGrav 15-year data. *Phys. Rev. D* **108**, 103511. (doi:10.1103/PhysRevD.108.103511)

49. Gouttenoire Y, Vitagliano E, 2023 Domain wall interpretation of the PTA signal confronting black hole overproduction. (doi:10.48550/arXiv.2306.17841)

50. Jiao H, Brandenberger R, Refregier A, 2023 Early structure formation from cosmic string loops in light of early JWST observations. *Phys. Rev. D* **108**, 043510. (doi:10.1103/PhysRevD.108.043510)

51. Peebles PJE, 2023 Flat patterns in cosmic structure. *Mon. Not. Roy. Astron. Soc.* **526**, 4490–4501. (doi:10.1093/mnras/stad3051)

52. Sanyal S, 2022 Nambu Goto cosmic strings in the early Universe. *Eur. Phys. J. Spec. Top.* **231**, 83–89. (doi:10.1140/epjs/s11734-021-00359-8)

53. Wang Z, Lei L, Jiao H, Feng L, Fan Y, 2023 The nanohertz stochastic gravitational-wave background from cosmic string Loops and the abundant high redshift massive galaxies. *Sci. China Phys. Mech. Astron.* **66**, 120403. (doi:10.1007/s11433-023-2262-0)

54. Tully RB, Howlett C, Pomarède D, 2023 Ho'oleilana: an individual baryon acoustic oscillation? *Astrophys. J.* **954**, 169. (doi:10.3847/1538-4357/aceaf3)

55. Einasto M, Heinämäki P, Liivamägi LJ, Martínez VJ, Hurtado-Gil L, Arnalte-Mur P, Nurmi P, Einasto J, Saar E, 2016 Shell-like structures in our cosmic neighbourhood. *Astron. Astrophys.* **587**, A116. (doi:10.1051/0004-6361/201526769)

56. Planck Collaboration, 2016 Planck 2015 results. XIII. Cosmological parameters, *Astron. Astrophys.* **594**, A13. (doi:10.1051/0004-6361/201525830)

57. Anderson L *et al.* 2014 The clustering of galaxies in the SDSS-III Baryon Oscillation Spectroscopic Survey: baryon acoustic oscillations in the data releases 10 and 11 galaxy samples. *Mon. Not. Roy. Astron. Soc.* **441**, 24–62. (doi:10.1093/mnras/stu523)

58. Eisenstein DJ *et al.* 2005 Detection of the baryon acoustic peak in the large-scale correlation function of SDSS luminous red galaxies. *Astrophys. J.* **633**, 560–574. (doi:10.1086/466512)